Robustness investigation of Horizontal Bidirectional Hybrid Damping System applied to long-span bridges under near-fault pulse-like earthquakes

Terms of use:

Publisher copyright

(Article begins on next page)

27 July 2024

Robustness investigation of Horizontal Bidirectional Hybrid Damping System applied to long-span bridges under near-fault pulse-like earthquakes

Renkang Hu [a,b], Menggang Yang [a], Dongliang Meng [a,**], Raffaele Cucuzza [b], Marco Domaneschi [b,*]

[a] *School of Civil Engineering, Central South Uiversity, Changsha, 410075, China*
[b] *Department of Structural, Geotechnical and Building Engineering, Politecnico di Torino, Turin, 10129, Italy*

ARTICLE INFO

ABSTRACT

This paper introduces a new integrated Horizontal Bidirectional Hybrid Damping System (HBHDS) incorporating eddy current dampers, metallic yielding dampers, fuse-lock device with a spherical steel bearing, for controlling the longitudinal and transverse vibrations of long-span bridges under near-fault pulse-like earthquakes. Based on the nonlinear time history analysis, the seismic response of a long-span bridge with HBHDS is investigated under different near-fault pulse-like earthquakes and compared to the installed damping system on the as-built bridge. The numerical results indicate that the HBHDS is an effective damping system against the near-fault earthquakes and exhibits a common tendency with similar or even better reductions of structural responses in comparison to installed damping system. Besides, a series of robustness investigations for HBHDS are carried out considering the out-of-service different HBHDS' components. It is found that HBHDS presents superior robustness to considering out-of-service dampers in terms of response reduction and energy dissipation capacity.

1. Introduction

As lifeline facilities to span the natural or man-made obstacles, long-span bridges play a vital role in the transportation network. Yet, their low damping ratio and large flexibility make those structures vulnerable to hazard environments such as earthquakes, particularly near-fault (NF) earthquakes [1]. The NF earthquake, as a typical pulse-like ground motion, is characterized by a high amplitude ground velocity and a long-duration pulse, which is caused by the forward-directivity (F-D) effect in the fault-normal direction and the fling-step (F–S) effect in the fault-parallel direction [2]. As a result, engineering structures subjected to NF earthquakes might experience the higher seismic responses and more severe damages compared to those under far-fault (FF) ground motions [3,4]. The bridges are liable to exceed the designed response limits, which may further lead to damage or failure affecting their functionality and safety. In the past, the damage or failure of bridges in NF seismic events have been reported, such as the Northridge Earthquake in 1994, ChiChi Earthquake in 1999, Wenchuan Earthquake in 2008, and Nepal earthquake in 2015 [5–8]. Thus, it is of great significance to seek and develop advanced damping techniques to protect the long-span bridges against NF earthquakes.

To control the undesirable responses of long-span bridges posed by NF earthquakes, the researchers have been devoted to exploiting the economic and easy-to-implement passive control techniques for energy dissipation [9]. Among them, fluid viscous dampers (FVDs) and metallic yielding dampers (MYDs) are typical displacement-dependent and velocity-dependent devices, respectively, which are widely employed in bridge engineering [10,11]. However, limitations have been found in applying FVDs and MYDs for seismic control of long-span bridges under NF ground motions. Specifically, FVDs may provide excessive damping forces to increase the tower internal forces of the bridge when experiencing NF earthquakes [12]. Moreover, damage or even failure of FVDs may occurs because they are sensitive to velocity pulses of NF earthquakes [13,14]. MYDs, due to their supplemental structural stiffness, may affect the structural dynamic characteristics, which also may have a negative influence on the seismic reduction [15].

The hybrid damping system, consisting of two or more damping devices combined together to form a single device, or managed in parallel/series connection, represents an effective approach by exploiting individual advantages and compensating their weakness [16,17]. It has

---

been proved to be a reliable seismic protective system and was practically applicable for bridges when experiencing NF earthquakes. For example, Liang et al. [18] combined FVDs and friction dampers in parallel to effectively control seismic-induced longitudinal displacement of a long-span suspension bridge. Hu et al. [19–21] experimentally and numerically studied a combined viscous-steel damping system (CVSDS) with FVD and MYD for long-span railway bridges subjected to seismic hazards. Compared with FVD and MYD, the CVSDS exhibits an excellent multi-level mitigation performance to reduce the longitudinal responses under NF earthquakes. Yi et al. [22] introduced a hybrid system incorporating negative stiffness device with FVDs for seismic reduction of long-span bridges under longitudinal NF earthquakes. The analytical results indicated the efficiency of the damping system is superior to that of individual damping device. Guan et al. [23,24] presented an effective lateral hybrid damping system for long-span cable-stayed bridges against NF earthquakes, which consists of elastoplastic cables and a parallel FVD. It is found that the system can achieve significant isolation effectiveness and energy dissipation. A transverse steel damper seismic system (TSDSS), including one transverse steel damper in parallel with two sliding spherical steel bearings, was proposed by Zhou et al. [25]. The distinct seismic isolation efficiency of TSDSS for long span cable-stayed bridges under NF ground motions were verified by a series of experiments. Besides, some new generation of hybrid systems for bridge applications, such as the shape memory alloy wire-based lead rubber bearings [26], U-shaped steel dampers in parallel with high damping rubber bearings [27], and tuned mass damper inerter in seismic response mitigation of base-isolation bridges [28] were also proposed to improve their seismic performance when subjected to NF earthquakes.

The above studies exploited the hybrid damping techniques for bridge's protection against NF earthquakes showing their effectiveness and feasibility to control the structural vibrations. However, these studies only focused on mitigating the longitudinal or transverse seismic responses. Furthermore, they also encountered challenges in addressing issues such as FVD damage malfunction resulting from fluid leakage [29, 30]. To this end, the authors developed a novel integrated hybrid system, referred to as Horizontal Bidirectional Hybrid Damping System (HBHDS), with multi-level vibration control capability for long-span bridges [31]. It consists of several components, i.e., eddy current dampers (ECDs), MYDs, fuse-lock devices (FLDs), and a spherical steel bearing (SSB). Focusing on ECD, being not susceptible to fluid phenomenon, it is used by replacing the traditional FVD to improve the reliability and durability of HBHDS and mitigate the responses caused by low-intensity earthquakes, while MYD is adopted to mitigate structural responses under strong earthquakes both in the longitudinal and transverse directions. An FLD mounted between the ECD and MYD plays a role of switch to realize that two dampers can work respectively as expected. A theoretical feasibility study of HBHDS has been carried out, encompassing its mechanical characteristics, parameter design, and effectiveness in mitigating under service loads and artificial ground motions.

This paper extends the findings of [31], investigating the robustness of HBHDS when applied to long-span bridges under different NF pulse-like earthquakes (F-D, F–S and non-pulse earthquakes). The organization of this paper is as follows: Section 2 presents a brief description of HBHDS to reveal its working mechanism and modeling. A long-span bridge equipped with different damping systems is introduced at Section 3, and the corresponding finite element (FE) model is established adopting the ANSYS FE code. Nonlinear time history analyses are performed under a set of recorded NF earthquakes with different pulse-like types at Section 4, and structural responses in terms of girder-tower displacements, bending moments and force-deformation relationship of the damping system are obtained. Section 5 discusses the robustness of HBHDS considering the out-of-service dampers of HBHDS' components under F-D pulse-like excitations. Finally, conclusions are summarized at Section 6.

2. Description of HBHDS

The hybrid damping system considered in this paper is shown in Fig. 1, which aims to mitigate the horizontal bidirectional response of long-span bridges when subjected to different intensities seismic excitations. It is composed of ECDs, MYDs, FLDs, and an SSB. The working principle of the system is elaborated as following.

In the longitudinal direction, ECDs and MYDs are in series through the FLD and mounted in parallel with SSB. FLD plays a role of a switch which can change the working status of HBHDS depending on the output damping force of ECD (F_{ECD}). In other word, ECD will alone dissipate energy by generating the eddy current-damping torque due to the relative motions between the conductors and permanent magnets as its output damping force is no more than the designed locking force of FLD (F_{Lock}). In this case, the inactivate FLD and the MYD with large stiffness can be considered as a rigid link and a fixed end, respectively. On the contrary, the FLD will be triggered when the F_{ECD} is greater than the F_{Lock} under strong earthquakes. Consequently, MYD will start to dissipate energy instead of ECD. In this case, FLD and ECD are equivalent to a rigid link since the movable plate of FLD will be connected to the shell of ECD (see Fig. 1(e)). It is worth to underline how the feasibility of FLD has been also verified by a series of tests [20,21].

In the transverse direction, the MYD component can simultaneously mitigate the bridge response in both the longitudinal and transverse directions under strong earthquakes. More specifically, the steel blocks welded to the top plate of SSB will transfer the inertial force to the top plate of MYD, because of the relative movement between the superstructure and the substructure, and then it will restraint the relative motion. To allow the free MYD motion in the longitudinal direction, a reasonable small gap between the steel blocks and the MYD is designed.

To further reveal the working principle of HBHDS, the force-displacement relationships are obtained by numerical finite element simulations under longitudinal and transverse harmonica loads, respectively. As shown in Fig. 2(a), different hysteretic loops are observed in the longitudinal direction. It means the ECD and MYD dissipate energy respectively due to the triggered FLD. In the transverse direction, only the stable hysteretic loop is presented in Fig. 2(b). This is because only MYD and SSB are working as expected. The more basic configuration and mechanical model details of the proposed hybrid system can be referred to Ref. [31].

3. Description and finite element modeling of the long-span bridge

The long-span bridge adopted as case study in the present study is the Sutong cable-stayed bridge in Jiangsu, China. It is a symmetrical bridge with a 1088 m main span and two 300 m side spans. The two reinforced concrete towers (34.5 MPa compressive strength) have an inverted-Y shape and a height of 300.4 m. The streamlined closed steel box girder (345 MPa yield strength) is used for wind resistance which is 41 m wide and 4 m high at central span. The overall layout of this bridge is shown in Fig. 3. To control the seismic longitudinal responses, four nonlinear FVDs have been installed at each tower-deck connections of the as-built bridge in the longitudinal direction [32]. In the transverse direction, wind-resistance bearings are employed for limiting the transverse displacements, which can be simplified as the fixed system (FS). In this study, as an alternative seismic protection system, two set of proposed HBHDS were installed at each tower-deck connection to mitigate the longitudinal and transverse responses. Moreover, the uncontrolled configuration of the bridge has been considered, i.e., free constraints are defined in the longitudinal and transverse direction at the tower-deck connections.

A full three-dimensional finite element (FE) model of the long-span bridge was established based on ANSYS FE code [33]. As illustrated in Fig. 4, the girder, piers and towers were simulated with the simple elastic beam elements Beam 4. The cables were modeled by tension-only
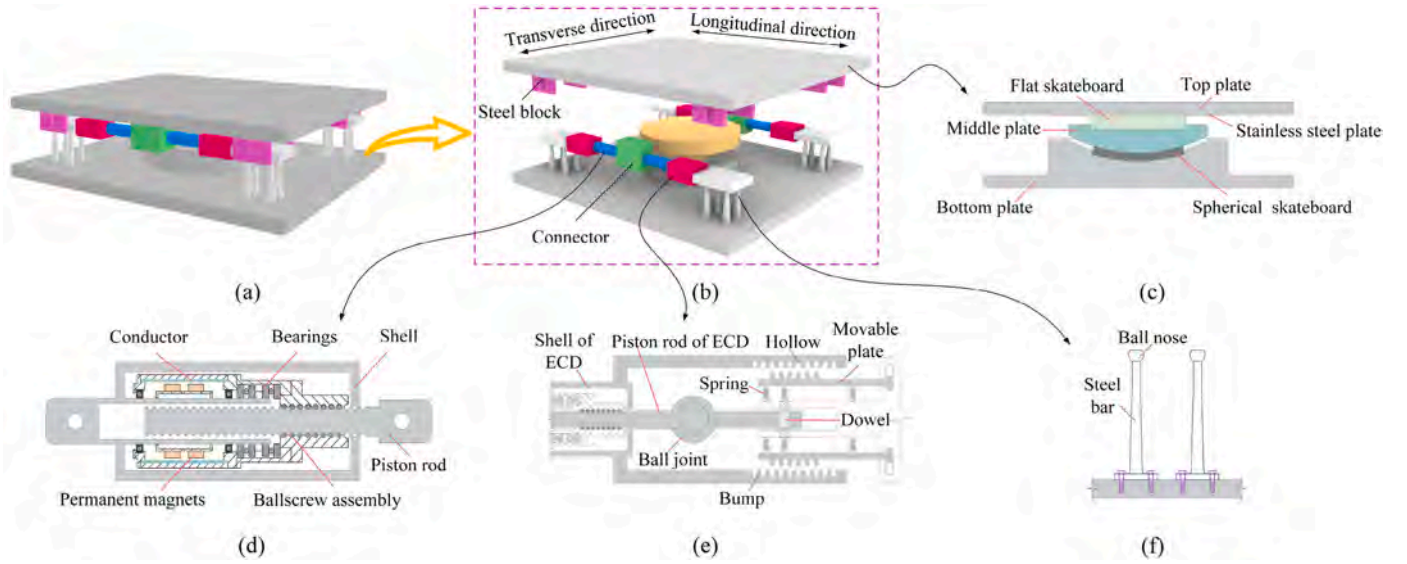
Fig. 1. Configuration of HBHDS: (a) the assembled HBHDS, (b) separated HBHDS, (c) SSB, (d) ECD, (e) FLD, and (f) MYD.

Fig. 2. The force-displacement relationship of HBHDS in the (a) longitudinal direction and (b) transverse direction.

truss element Link 10 element using the Ernst method [34]. The nonlinear components of the model are therefore concentrated to the characteristics of the devices implemented for the various bridge configurations and on the modeling of the stay-cables as tension-only elements. Fixed base conditions were defined and the soil-structure interaction is not considered. The FE model of the case study consists of 870 nodes and 1156 elements. The inherent damping ratio (3 %) was defined by a Rayleigh damping distribution. Note that the model is developed by directly defining the nodes connected by the elements with suitable boundary conditions. The first six vibration modes of the FE bridge model are plotted in Fig. 5. They are in good agreement with the results displayed in Ref. [35].

The HBHDS' components have been modeled as follows: the bilinear model [36] was used to reproduce the MYD and SSB in the system, as shown in Fig. 4. Due to the absence of element in ANSYS for ECD, its nonlinear force-velocity behavior was represented by utilizing the F_{ECD} obtained by the classic Wouterse model [37] (see Eq. (1)) during each iteration, and which is subsequently applied to the relevant connected elements. Note that the feasibility and accuracy of this model to characterize such ECD's mechanical behavior were validated by experiments and simulations [38].

$$F_{ECD} = 2F_{max} v_{cr} v / \left(v_{cr}^2 + v^2 \right) \qquad (1)$$

where F_{max} is the maximum damping force, v_{cr} is the critical relative velocity, v is the girder-tower relative velocity. Besides, the function of FLD can be reproduced by comparing the F_{ECD} with the F_{Lock} in each iteration. Once the F_{ECD} is larger than the F_{Lock}, the MYD's elements will be directly connected between the tower and girder, whereas the F_{ECD} is

not applied. The FVD's hysterical behavior can be modeled by Eq. (2) and simulated by the element Combin 37 [39].

$$F_{FVD} = C \mathrm{sgn}(v) v^\alpha \qquad (2)$$

where C is the damping coefficient, α is the velocity exponent. All the design parameters of the adopted damping systems are summarized in Table 1. More details for how to obtain these design parameters of HBHDS and FVD can be refereed to Refs. [31,32].

4. Robustness analyses in structural responses with HBHDS under near-fault pulse-like earthquakes

4.1. Selection of near-fault earthquakes

NF pulse-like ground motions, in comparison to non-pulse NF and FF ones, show different characters with a high amplitude ground velocity and a long-duration pulse because of F-D and F–S effects [2,40]. Here, according to the Specifications for Seismic Design of Highway Bridges in China [41], a total of nine NF earthquakes (including three F-D, three F–S and three non-pulse-like earthquakes) are taken as examples from the Pacific Earthquake Engineering Research Center database and the near-source ground-motion datasets [42]. Table 2 lists the main information and characteristics of those ground motions such as the peak ground velocities PGVs, moment magnitude M_w, distance to fault rupture R_{rup}, and pulse period T_p. Fig. 6 shows the individual acceleration spectrum of nine NF ground motions along with their mean spectrum. The acceleration and velocity time histories of three typical NF pulse-like ground motions (GM 1, GM 4 and GM 7) are plotted in Fig. 7. It can be observed how that the GM 1 (see Fig. 7(a)) contains
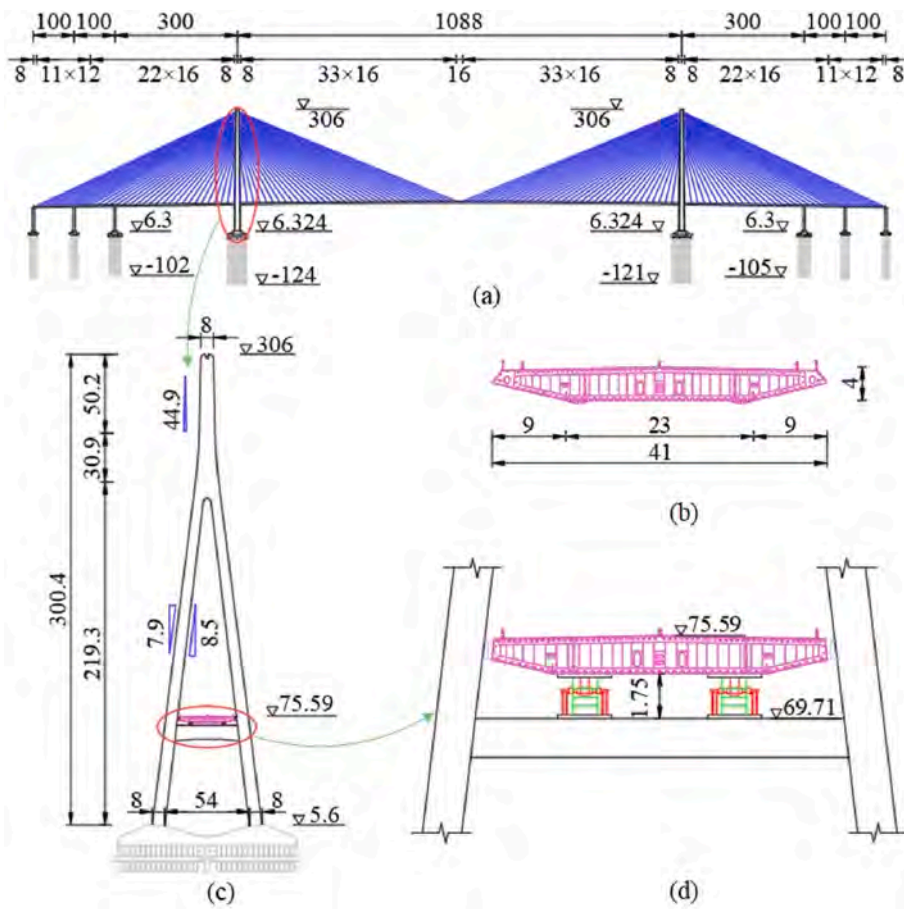
Fig. 3. Configuration of the long-span cable-stayed bridge (Unit: m): (a) elevation of the bridge, (b) geometry of the box girder, (c) geometry of the tower, and (d) location of HBHDS.
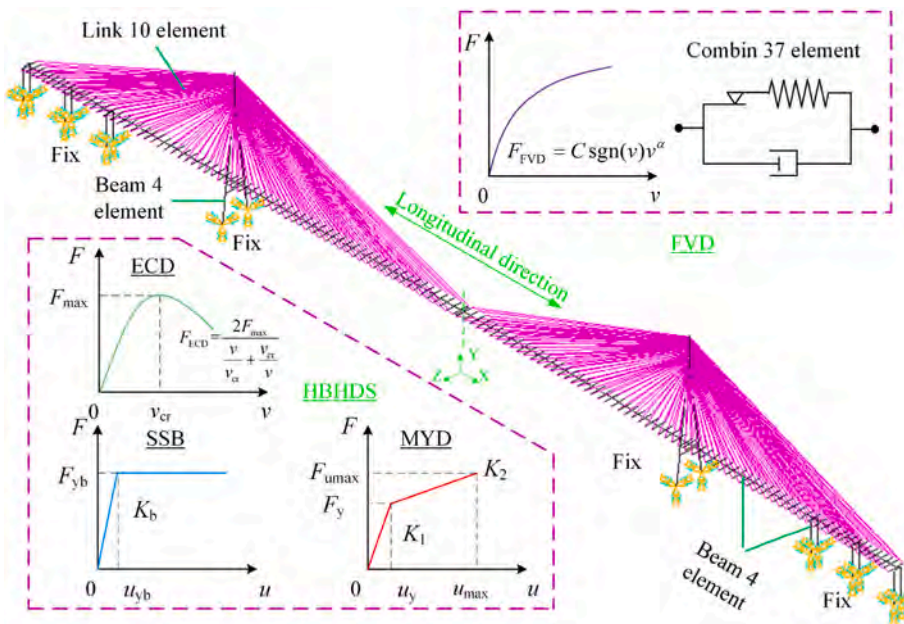

Fig. 4. Configuration and finite element model of the long-span bridge.

multi-velocity pulses when compared with GM 4 (see Fig. 7(b)) due to the effect of the fault rupture mechanism [43]. It should be noted that the influence of vertical ground motion is neglected and the peak ground accelerations of the selected seismic records were scaled to a peak value of 0.25 g before inputting them (separately) to the FE model in the longitudinal and transverse directions. It is also worth noting that the
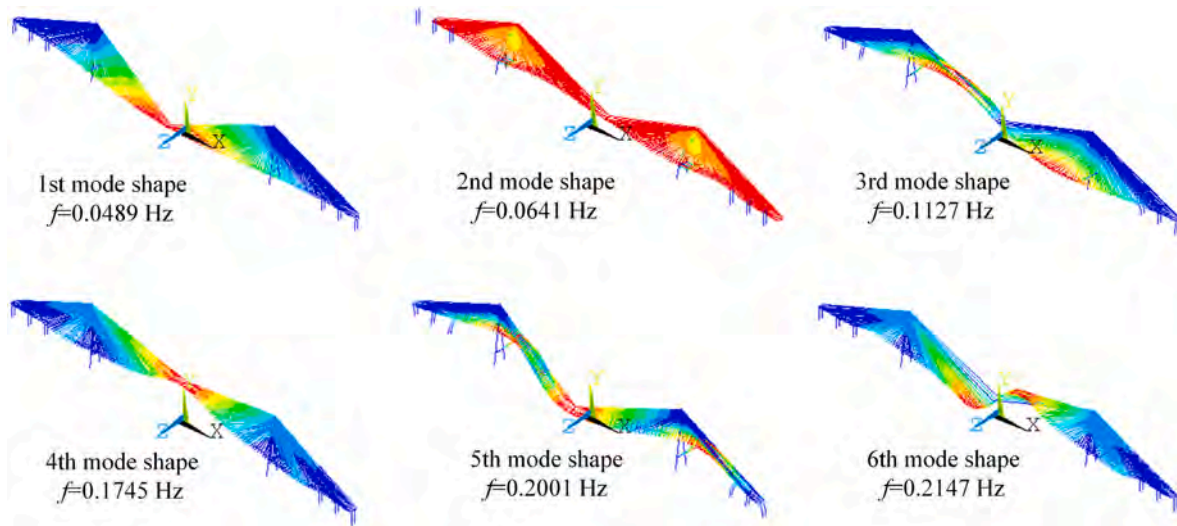
Fig. 5. The first 6 mode shapes of the bridge model (uncontrolled version).

Table 1
The mechanical parameters of each component in different damping system.

Damping system	Component	Parameters	
FVD	FVD	C (kN·(s/m)$^{0.4}$)	3750
		α	0.4
HBHDS	ECD	F_{max} (kN)	1090
		v_{cr} (m/s)	0.40
	MYD	u_y (m)	0.025
		u_{max} (m)	0.35
		K_1 (kN/mm)	47.4
		K_2 (kN/mm)	1.88
	SSB	u_{yb} (m)	0.002
		F_{yb} (kN)	24
	FLD	F_{Lock} (kN)	1035

Table 2
Main information of near-fault pulse-like ground motions used in this study.

No.	Year	Earthquake name	Mw	Rrup (km)	PGV (cm/s)	Tp (s)	Pulse type
GM1	2010	Darfield	7.0	8.46	38.13	7.826	F-D
GM2	1999	Chi-Chi, TCU051	7.62	6.95	54.89	10.38	F-D
GM3	1989	Loma Prieta	6.93	11.07	41.84	1.23	F-D
GM4	1979	Imperial Valley-06	6.53	10.42	46.40	4.396	F–S
GM5	1999	Chi-Chi, TCU075	7.62	0.89	116.2	4.998	F–S
GM6	1999	Kocaeli_Turkey	7.51	1.38	71.86	4.949	F–S
GM7	1940	Imperial Valley-02	6.95	6.09	31.33	–	None
GM8	1999	Chi-Chi, KAU050	7.62	5.19	4.44	–	None
GM9	1999	Chi-Chi, TCU059	7.62	8.51	14.32	–	None

Fig. 6. Spectra acceleration versus time period for 9 near-fault ground motions.

Moreover, the structural responses with FVDs employed to the actual bridge are also obtained and compared with HBHDS to further reveal the robustness of HBHDS. Fig. 8 depicts the configurations of the bridge without control (Fig. 8(a)) and with different damping systems (Fig. 8 (b)). Note that there is no any constraint in Fig. 8(a) between the deck and tower.

4.2.1. Girder-tower relative displacement

Fig. 9 shows the girder-tower relative displacement (D_L) time histories of the long-span bridge equipped with and without HBHDS or FVD under different NF pulse-like ground motions in the longitudinal direction. The corresponding maximum values of D_L (D_{L-max}) and reduction ratios are listed in Table 3. As shown, the HBHDS and FVD can significantly mitigate the maximum dynamic responses of the bridge under all seismic excitations. Moreover, the proposed HBHDS shows the similar or even better response control effect comparing to the FVD installed in the as-built bridge.

Taking the case wherein the bridge is subjected to GM 1, the D_{L-max} of the uncontrolled bridge is 0.687 m, while they are 0.333 m and 0.349 m in the cases with HBHDS and FVD, as shown in Fig. 9(a). The corresponding reduction ratios are 51.6 % and 49.2 %, respectively. When subjected to the NF earthquake without pulse (GM 7), the D_{L-max} values are 0.184 m, 0.115 m and 0.149 m for the three cases, and the reduction rations of D_{L-max} are respectively 37.8 % and 19.1 % for HBHDS and FVD. These numerical results illustrate that the structural displacement responses due to NF pulse-like ground motions with pulses are larger

relationship between pulse periods and structural responses has been investigated. However, it has been found to be negligible, in agreement with what has already been reported in the literature, e.g. [44].

4.2. Seismic response under longitudinal near-fault pulse-like earthquakes

When subjected to three different typical NF pulse-like motions, structural responses in terms of girder-tower relative displacement, bending moment at the base of the bridge tower and force-deformation relationship of the damping system are investigated.
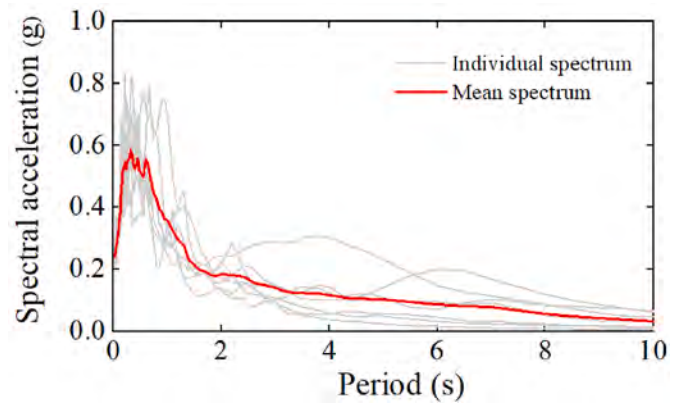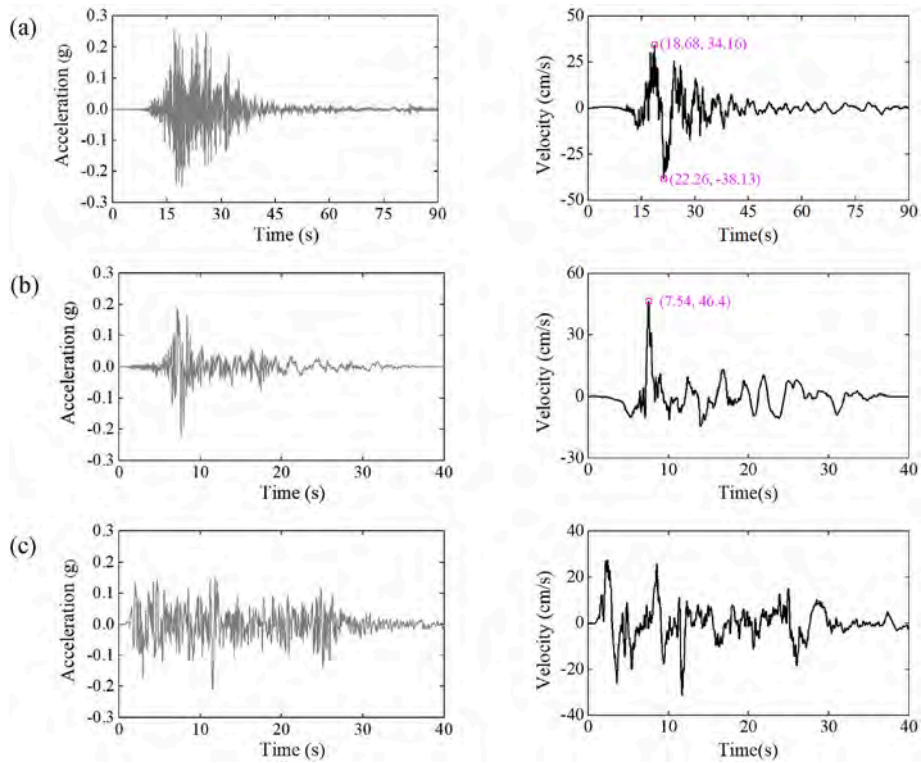
Fig. 7. The acceleration and velocity time histories of the input NF ground motions: (a) GM 1 with F-D effect, (b) GM 4 with F–S effect and (c) GM 7 with non-pulse effect.
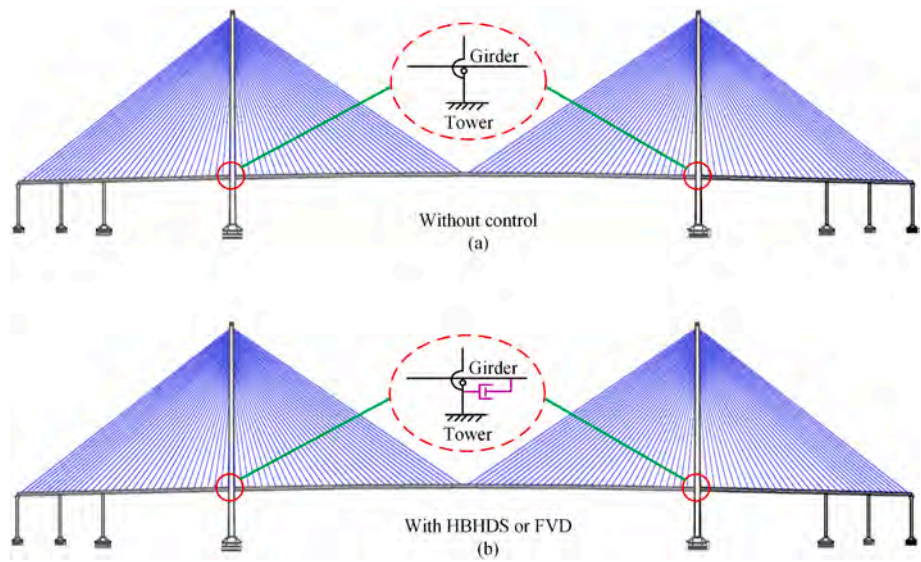

Fig. 8. Configurations of the bridge with different damping systems.

than those ones generated by the NF ground motion without pulse.

It should be noted that FLDs in HBHDS are triggered at 21.02 s under GM 1, which is preceding to the time of maximum velocity pulse at 22.26 s (see Fig. 7 (a)). In other word, the ECD will quit working due to the activation of FLD, and MYD will play the dominant role in dissipating the seismic energy. Similar to what happened under GM 1, the triggered time of FLDs is preceding to the time of maximum velocity pulse under GM 4. On the contrary, FLDs are not triggered under GM 7, meaning that ECD will play the dominant role in dissipating the seismic energy. The fuse-locking mechanism will be further discussed and illustrated in next section.

4.2.2. Bending moment at the base of the bridge tower

The bending moment (M_L) time histories at the base of the bridge tower of the long-span bridge equipped with and without HBHDS or FVD under different NF pulse-like ground motions in the longitudinal direction are shown in Fig. 10. Compared to the significant reductions in girder-tower displacement responses, relatively small decreases even slight increases are observed in the bending moment responses, as summarized in Table 4. Specifically, when subjected to the F-D pulse-like seismic excitation (GM 1), the maximum values of M_L ($M_{L\text{-max}}$) for the bridge with damping systems are 975563 (with HBHDS) and 831012 **kN·m** (with FVD), and the reduction ratios are respectively 10.8
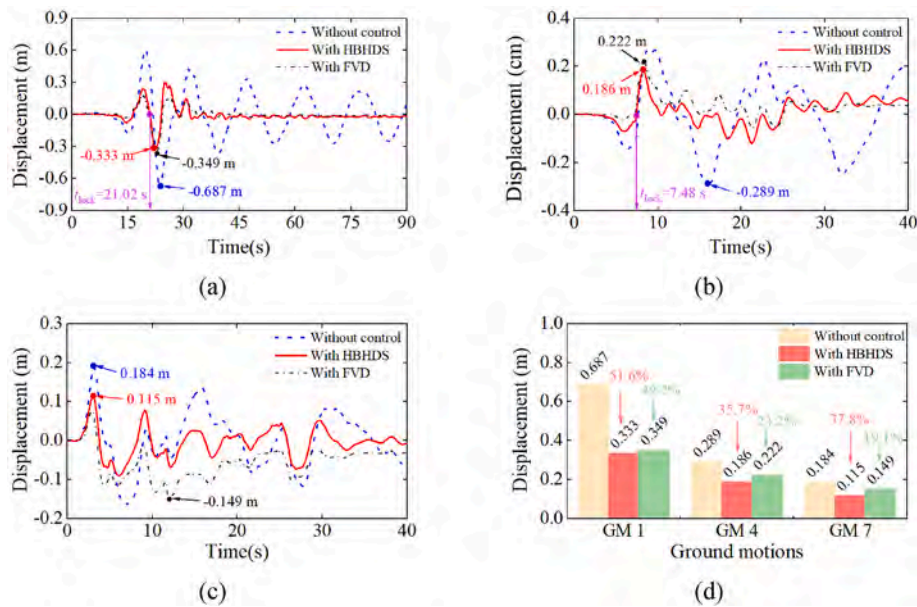
Fig. 9. Mitigation effects of HBHDS and FVD on the girder-tower relative displacements of the bridge under different near-fault ground motions in the longitudinal direction: (a) GM 1, (b) GM 4, (c) GM 7 and (d) maximum girder-tower relative displacements.

Table 3
Maximum girder-tower displacements and the corresponding reduction ratios in the longitudinal direction.

Ground motions		Maximum girder-tower displacement (m)			Reduction ratio (%)	
		Uncontrol	HBHDS	FVD	HBHDS	FVD
F-D	GM1	0.687	0.333	0.349	51.6	49.2
	GM2	0.228	0.129	0.094	43.4	58.8
	GM3	0.274	0.118	0.086	56.9	68.6
F–S	GM4	0.289	0.186	0.222	35.7	23.2
	GM5	0.498	0.274	0.232	50.0	53.4
	GM6	0.282	0.241	0.264	14.9	6.5
Non-pulse	GM7	0.184	0.115	0.149	37.8	19.1
	GM8	0.347	0.196	0.246	43.5	29.1
	GM9	0.383	0.174	0.145	54.6	62.1

% and 24.0 % comparing with the uncontrolled case. However, the HBHDS and FVD have an adverse effect on $M_{L\text{-max}}$, which slightly increases in the range of 4.6–32.2 % and 17.1–25.1 % due to the F–S pulse-like and non-pulse-like ground motions. This is probably due to the dynamic characteristics of the input seismic excitations and the excessive supplemental damping generated by the velocity-dependent dampers (ECDs in HBHDS and FVDs), which is proved to be detrimental for structures [22,42]. Although the slight increase of structural bending moments may be undesired, the pronounced mitigation in displacement responses make it satisfactory.

Furthermore, the proposed HBHDS has resulted in the common tendency with similar reductions of bending moments at the base of the bridge tower compared to the cases where FVDs were applied to the actual bridge. The difference in reduction ratio between them is approximately 10 %. These conclusions are also in consistent with those in the analyses of structural girder-tower displacement responses. It suggests that novel HBHDS can be serve as an alternative to FVDs as they can provide the better mitigation effect on structural responses.

4.2.3. Force-displacement relationship

The force-displacement relationships of HBHDS and FVD applied to the long-span bridge under F-D pulse-like NF earthquakes in the longitudinal direction are presented in Fig. 11. In detail, Fig. 11(a) displays the force time histories of each ECD in one set of HBHDS. It is clearly

observed that the output damping force of ECD is zero after 21.02 s. This is because the damping force of ECD reaches the locking force 1090 kN and the FLD is triggered. In other hand, the activated FLDs switch the operating status of ECD and MYD, i.e., ECD quits working while MYD begins to dissipate energy following this time instant. As a result, different force-displacement relationships are shown in Fig. 11(b), in which the lines in blue and red represent the hysteretic loop of ECD and MYD in HBHDS, respectively. This can further reveal the working mechanism of the proposed damping system. It should be noted that the output force of ECD is 1030 N at 21.02 s, which is less than the design locking force. However, it will reach the design value in the next iteration during the nonlinear time history analysis, then the FLD will be triggered. Consequently, the ECD is protected from damage or failure due to the excessive force induced by NF ground motions.

The larger maximum output force and associated hysteretic loops can be observed for the FVD in Fig. 11(c)–(d), in comparison to ECD as illustrated in Fig. 11(a)–(b). It represents the greater damping force should be designed for the single FVD than ECD, which will result in the higher risk of damage to local components of the structures [22].

The force-displacement relationships of HBHDS and FVD in the long-span bridge under F–S pulse-like NF earthquakes in the longitudinal direction is illustrated in Fig. 12. Similar to the results under GM 1, MYD plays the dominant role in dissipating energy due to the function of the FLD. However, focusing on non-pulse NF ground motion (Fig. 13), the evident discrepancies can be observed in the force-displacement relationship of the HBHDS compared to the results shown in Figs. 11 and 12. Since the different ground motion characteristics of GM 7, the maximum damping force of ECD is 950 kN, which is much less than the design locking force. It means the FLD has not been activated and ECD in HBHDS plays the dominant role in dissipating the seismic energy. Both the hysteretic loops can be observed in Fig. 13 (b) and (d) respectively for HBHDS and FVD when experiencing a non-pulse NF ground motion.

The results indicate that the HBHDS can not only dissipate the NF pulse-like seismic energy to control the structural responses as effectively as FVD, but also reduce output force of FVD and then alleviate the structural damage or failure.

4.3. Seismic response under transverse near-fault pulse-like earthquakes

Similar to Section 4.2, the mitigation effectiveness of HBHDS under
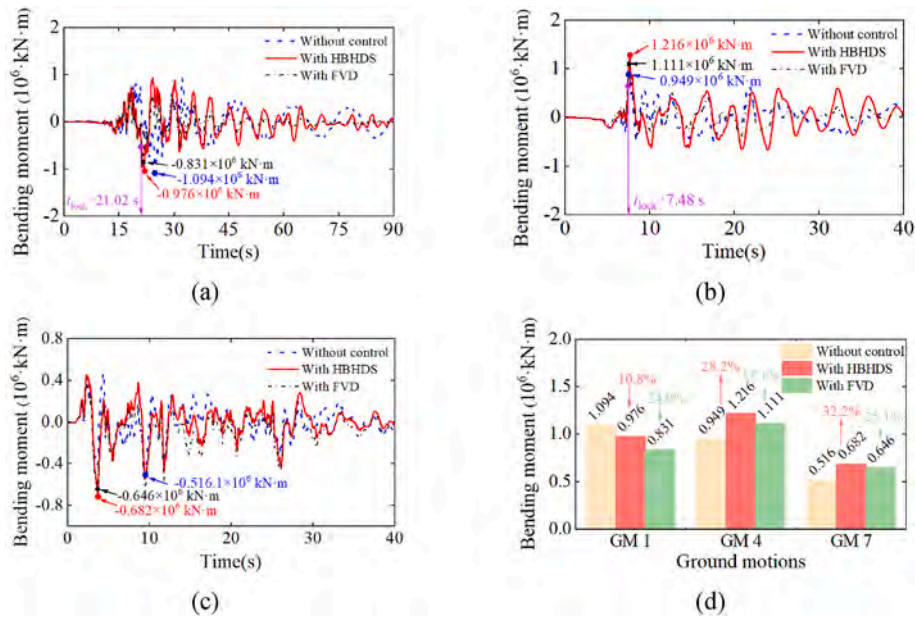
Fig. 10. Mitigation effects of HBHDS and FVD on the bending moment at the base of the bridge tower under different near-fault ground motions in the longitudinal direction: (a) GM 1, (b) GM 4, (c) GM 7 and (d) maximum bending moments.

Table 4
Maximum bending moments at the base of the bridge tower and the corresponding reduction ratios in the longitudinal direction.

Ground motions		Maximum Bending moment (10^6 kN·m)			Reduction ratio (%)	
		Uncontrol	HBHDS	FVD	HBHDS	FVD
F-D	GM1	1.094	0.976	0.831	10.8	24.0
	GM2	1.497	1.054	0.699	29.5	53.3
	GM3	1.551	0.765	0.769	50.7	50.4
F–S	GM4	0.949	1.216	0.682	−28.2	−17.1
	GM5	0.732	0.767	0.601	−4.6	18.0
	GM6	0.909	0.862	0.639	5.2	29.7
Non-pulse	GM7	0.516	0.682	0.646	−32.2	−25.1
	GM8	0.835	0.772	0.801	7.6	4.2
	GM9	0.671	0.557	0.483	17.0	28.1

transverse NF pulse-like earthquakes is discussed at this section. In the as-built bridge, wind-resistance bearings are utilized for limiting the transverse displacements instead of the FVDs used to control the longitudinal responses, which can be simplified as the fixed system (FS). Additionally, to further illustrate the performance efficiency of HBHDS, the transverse constraints were also release in this study, i.e., structural responses with HBHDS and with FS are compared with those ones of the uncontrolled case.

4.3.1. Girder-tower relative displacement

The girder-tower relative displacement (D_T) time histories of the long-span bridge with HBHDS, without control and with FS under three NF ground motions in the transverse direction are presented in Fig. 14, and the maximum values of D_T are listed in Table 5. Compared with the reductions in longitudinal girder-tower displacements, more considerable decreases are observed in the transverse displacements, especially there is no transverse relative motions in the case of bridges with FS. The reduction ratios of HBHDS are in the range of 75.9%–92.7 %. These results illustrate that HBHDS can effectively control the transverse maximum responses of structures under all seismic excitations. Considering F-D pulse-like earthquake (GM 1) input, as an example, the maximum value of D_T decreases from the uncontrolled case of 0.291 m to the controlled case (with HBHDS) of 0.061 mm, with a reduction of 79.0 %.

4.3.2. Bending moment at the base of the bridge tower

Fig. 15 shows the bending moment (M_T) time histories at the base of the bridge tower of the long-span bridge equipped with and without HBHDS under different NF pulse-like earthquakes in the transverse direction. A similar behavior already observed in Fig. 10 for the longitudinal direction can be observed. Namely, installing the proposed damping system slightly increases the bending moment at the base of the bridge tower. The maximum value of M_T increases in the range of 4.1–38.9 % due to the supplemental stiffness provided by MYD in HBHDS, as listed in Table 6. It can be also proved by the transverse fundamental period of the bridge varying from 20.833 to 10.428 s after installing HBHDS. It should be noted that the values of M_T with fixed system is slightly larger than those ones equipped with HBHDS or without control. Therefore, it can be concluded that the proposed HBHDS can moderately mitigate bending moments at the base of the bridge tower compared with the transverse damping system (FS) adopted in the as-built bridge.

4.3.3. Force-displacement relationship

Fig. 16 shows the force-displacement relationships of HBHDS under three NF earthquakes in the transverse direction. The results illustrate the MYD dissipation of the input seismic energy by inelastic deformation. Besides, the shapes of hysteretic curves are different under the three NF earthquakes, which can be explained by the smaller transverse girder-tower displacements compared with the longitudinal displacements. The force-displacement relationships of HBHDS can also verify the working mechanism of HBHDS as expected in the transverse direction, i.e., the MYD in HBHDS dissipates most of the input seismic energy for mitigating the structural response in the transverse directions.

5. Robustness analyses considering the out-of-service dampers in HBHDS under near-fault pulse-like earthquakes

Robustness is a desirable property of structural systems to characterize the insensitivity of a structure to local failure. It is measured by a quantitative description which can be used not only for optimization design, but also for evaluation and regulation of robustness [45]. For example, Das et al. [46] utilized the robust design optimization to determine the tuning parameters of a new type of nonlinear controller. Domaneschi et al. [47] evaluated the robustness of a hybrid system
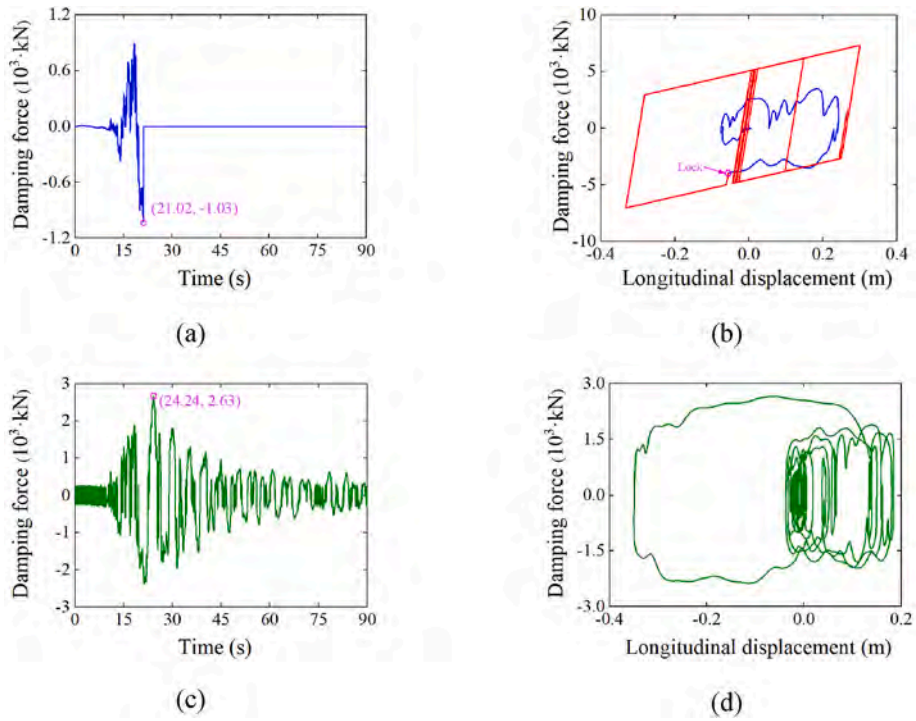
Fig. 11. The force-displacement relationships of HBHDS and FVD under GM 1 in the longitudinal direction.
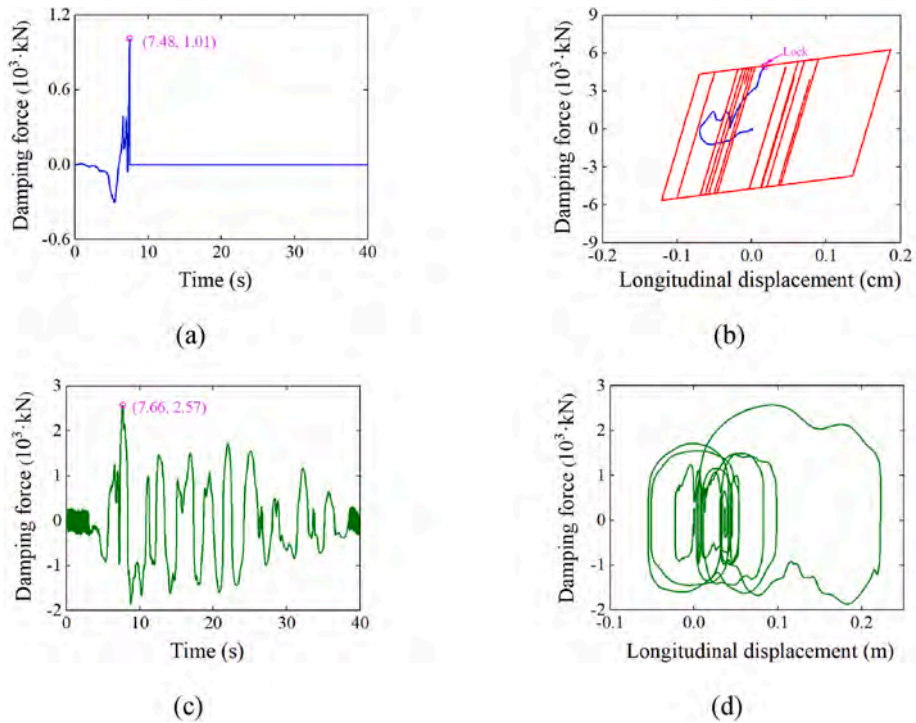

Fig. 12. The force-displacement relationships of HBHDS and FVD under GM 4 in the longitudinal direction.

implemented on a long-span suspension bridge considering out-of-service dampers in the system. In this work, the out-of-service dampers in HBHDS are also discussed to explored the robustness property of HBHDS under F-D pulse-like NF earthquake (GM 1). Note that when the out-of-service dampers occurs in one set of HBHDS, the same damage is assumed for the other HBHDS in this study since this will lead to the most adverse impact on the bridge response.

In the longitudinal direction, four cases considering the out-of-

service dampers in HBHDS are listed in Table 7. Specifically, case 1 represents all of the dampers in HBHDS are out of service (i.e., con-straints between deck and tower are completely released equivalent to without control), while case 2 represents the proposed HBHDS without any failure and fully working. For case 3, only ECDs in HBHDS are out of service, which means the bridge is controlled by MYDs and SSBs. Based on case 3, the failure of MYDs appears in case 4, namely only SSBs in HBHDS dissipate energy. It should be note that the out-of-service ECDs
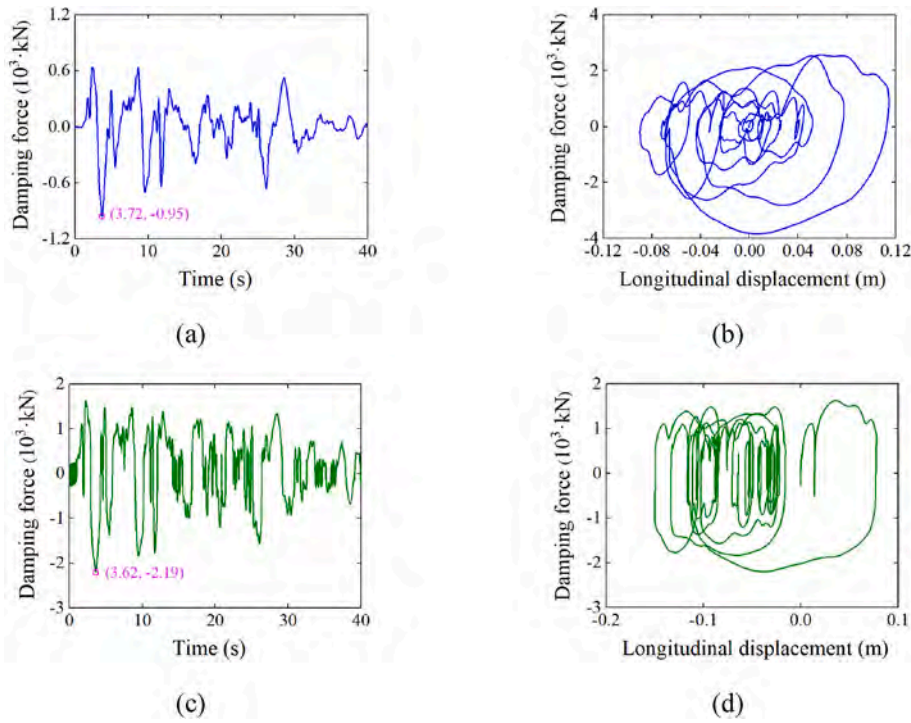
Fig. 13. The force-displacement relationships of HBHDS and FVD under GM 7 in the longitudinal direction.
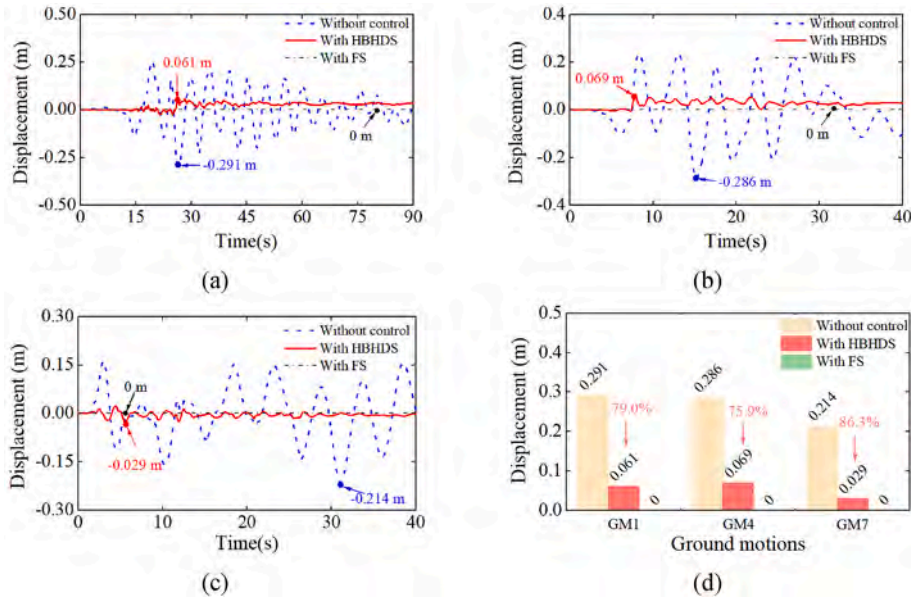

Fig. 14. Mitigation effects of HBHDS and FS on the girder-tower relative displacements of the bridge under different near-fault ground motions in the transverse direction: (a) GM 1, (b) GM 4, (c) GM 7 and (d) maximum girder-tower relative displacements.

and SSBs simultaneously are not considered since the HBHDS will fail to work without SSB.

In the transverse direction, SSBs and MYDs in HBHDS are expected to mitigate the seismic responses. Hence, three cases in total are analyzed and listed in Table 7 to further explore the robustness of HBHDS in the transverse direction, including out-of-service MYDs (case 1), out-of-service MYDs and SSBs simultaneously (case 2), and without any failure of dampers (case 3) in HBHDS. The robustness of HBHDS on the long-span bridge will be evaluated in terms of response reduction and energy dissipation capability under different cases in the following subsections.

5.1. Robustness comparison in terms of response reduction

5.1.1. Longitudinal direction

Fig. 17(a) and (b) compares the time histories of the structural responses in terms of girder-tower relative displacements and bending moments at the tower base for different control configurations in the longitudinal direction. It clearly appears that the HBHDS without any failure (case 2) can achieve the better control effect on D_L and M_L in comparison to other 3 cases, while the M_L in case 3 slightly increases.

The $D_{L\text{-max}}$ values for the four cases are summarized in Table 8, in which the corresponding reduction ratios of case 2–4 compared to case 1

Table 5
Maximum girder-tower displacements and the corresponding reduction ratios in the transverse direction.

Ground motions		Maximum girder-tower displacement (m)			Reduction ratio (%)	
		Uncontrol	HBHDS	FS	HBHDS	FS
F-D	GM1	0.291	0.061	0	79.0	100
	GM2	0.637	0.049	0	92.2	100
	GM3	0.559	0.045	0	92.0	100
F–S	GM4	0.286	0.069	0	75.9	100
	GM5	0.382	0.028	0	92.7	100
	GM6	0.388	0.029	0	92.6	100
Non-pulse	GM7	0.214	0.029	0	86.3	100
	GM8	0.363	0.072	0	80.2	100
	GM9	0.314	0.043	0	86.3	100

are also listed. It can be seen that HBHDS without any failures in case 2 exhibits the best control effects: $D_{\text{L-max}}$ and $M_{\text{L-max}}$ values are 0.333 m and 975563 kN·m, and the corresponding reduction ratios are 51.6 % and 10.8 %, respectively. It is worth noting that $D_{\text{L-max}}$ value in case 3 is 0.377 m, which is close to the result obtained in case 2, while the displacement exceeds the design value of 0.35 m in Ref. [31]. As a result, it can be concluded how HBHDS has the best robustness in terms of seismic responses among the cases considering the out-of-service dampers under the longitudinal NF pulse-like earthquakes.

5.1.2. Transverse direction

Fig. 18 shows a comparison in terms of D_T and M_T of the bridge between the uncontrolled bridge (out-of-service MYDs and SSBs simultaneously), the bridge with HBHDS (without any failure of dampers in HBHDS) and only the SSD (out-of-service MYDs). The $D_{\text{T-max}}$ and $M_{\text{T-max}}$ values for the three cases are listed in Table 9, in which the response reduction ratios are also illustrated. The HBHDS without any failure is proved effective for the transverse displacement although the bending moment reductions slightly increases compared to the out-of-service cases. In other words, the HBHDS displays the desirable robustness for controlling the structural responses when experiencing NF pulse-like earthquakes.

5.2. Robustness comparison in term of energy dissipation capacity

5.2.1. Longitudinal direction

Fig. 19(a) plots the time histories of the dissipated energy of HBHDS considering different out-of-service dampers under GM 1 in the longitudinal direction. It is evident that the bridge with HBHDS (case 2) and out-of-service ECDs in HBHDS (case 3) can significantly dissipate seismic energy than case 4. In case 2, the energy dissipated by HBHDS without any failure dampers is 8.631 MJ, which is slightly larger than 7.441 MJ dissipated by HBHDS with out-of-service ECDs in case 3. Moreover, a sharp increase in the dissipated energy is observed within a short time period from 15 to 23 s. This is because the time period is consistent to that of the velocity pulse (see Fig. 7(a)).

The bar chart of Fig. 19(b) shows the energy dissipated by the dampers in HBHDS. It is found that the energy dissipated by ECD, MYD and SSB is 1.651 MJ, 6.908 MJ and 0.072 MJ, respectively. The results illustrate that MYD plays the dominant role in dissipating seismic energy compared with ECD and SSB. This can further reveal the working principle of HBHDS introduced at Section 2, and verify its feasibility under NF pulse-like ground motions.
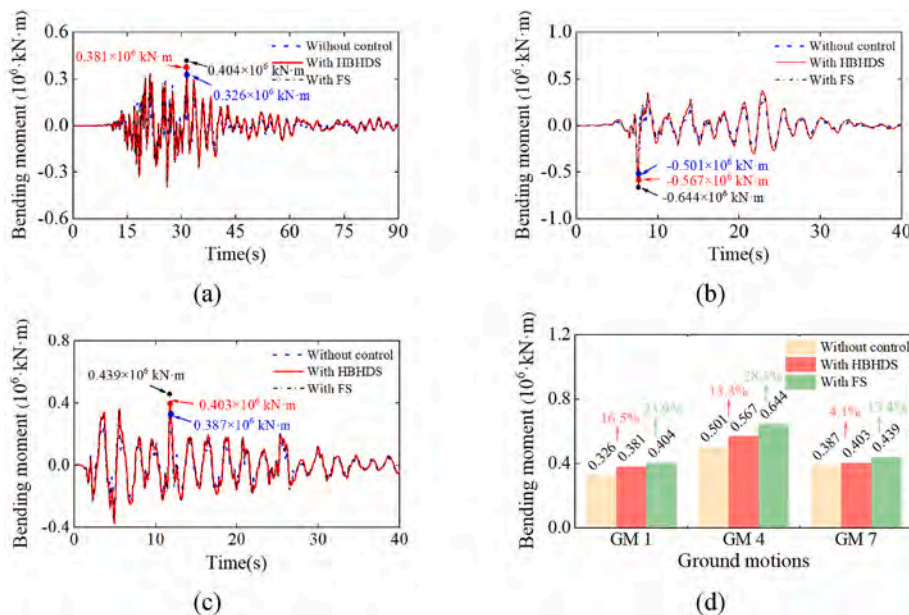
5.2.2. Transverse direction

Similar to Section 5.2.1, the dissipated energy by HBHDS considering different out-of-service dampers under the NF pulse-like earthquake in

Table 6
Maximum bending moments at the base of the bridge tower and the corresponding reduction ratios in the transverse direction.

Ground motions		Maximum Bending moment (10^6 kN·m)			Reduction ratio (%)	
		Uncontrol	HBHDS	FS	HBHDS	FS
F-D	GM1	0.326	0.381	0.404	−16.5	−23.9
	GM2	0.333	0.462	0.469	−38.9	−40.9
	GM3	0.486	0.559	0.627	−15.1 %	−29.1
F–S	GM4	0.501	0.567	0.644	−13.3	−28.5
	GM5	0.349	0.459	0.468	−31.5	−33.9
	GM6	0.395	0.506	0.513	−28.1	−29.9
Non-pulse	GM7	0.387	0.403	0.439	−4.1	−13.4
	GM8	0.434	0.524	0.537	−20.7	−23.6
	GM9	0.272	0.376	0.378	−38.1	−38.7

Fig. 15. Mitigation effects of HBHDS and FS on the bending moment at the base of the bridge tower under different near-fault ground motions in the transverse direction: (a) GM 1, (b) GM 4, (c) GM 7 and (d) maximum bending moments.
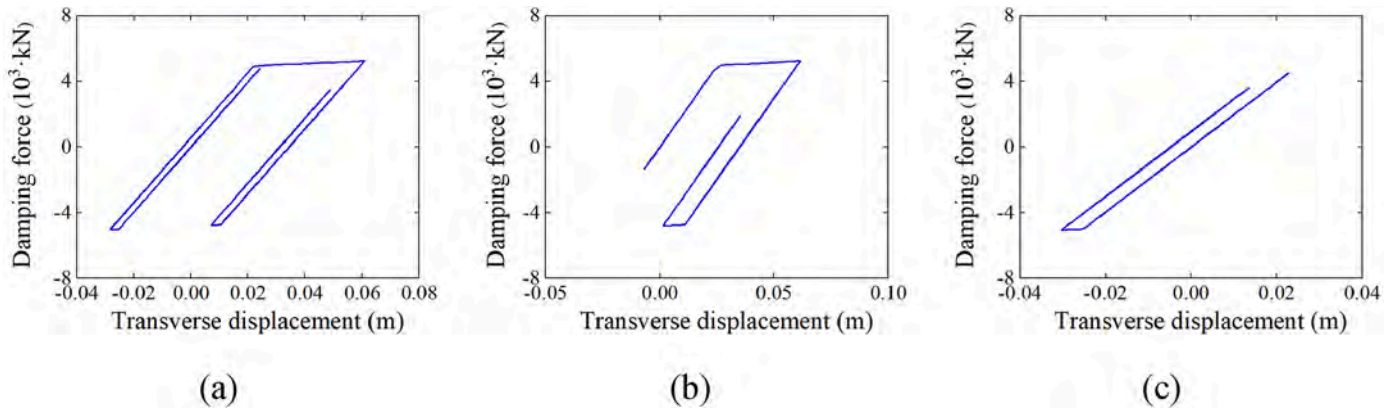
Fig. 16. The force-displacement relationships of HBHDS due to different NF ground motions in the transverse direction: (a) GM 1, (b) GM 4 and (c) GM 7.

Table 7
Cases of considering out-of-service HBHDS' components in the longitudinal and transverse directions.

Direction	Case	Out-of-service components in HBHDS
Longitudinal	1	Without control
	2	With HBHDS
	3	With MYD + SSB
	4	With SSB
Transverse	1	Without control
	2	With HBHDS
	3	With SSB

the transverse direction is obtained, as shown in Fig. 20. The HBHDS without failure can dissipate more energy than the case with out-of-service dampers in HBHDS, and the most of the seismic energy is dissipated by MYD as expected.

6. Conclusions

In this study, a new hybrid damping solution, referred as to Horizontal Bidirectional Hybrid Damping System (HBHDS), is developed to protect long-span bridges against different near-fault (NF) pulse-like earthquakes in the longitudinal and transverse directions. The mitigation effectiveness of the proposed hybrid system is investigated and compared with fluid viscous dampers (FVDs) installed in the as-built bridge. Robustness analyses are also performed to evaluate the feasibility and superiority of HBHDS under different cases considering the out-of-service dampers in HBHDS. The main conclusions are drawn as follows.

(1) Compared to the FVDs of the as-built bridge in the longitudinal direction, HBHDS exhibits similar or even better reductions of structural responses under different NF earthquakes. The girder-tower relative displacement reduction ratios of HBHDS and FVD are in the range of 14.9%–56.9 % and 6.5–68.6 %, while the bending moment at the base of the bridge tower are slightly increases in the range of 4.6–32.2 % and 17.1–25.1 %. This suggests that HBHDS can be serve as an alternative to the traditional FVD.

(2) In the transverse direction, HBHDS shows significantly vibration control effect with the reduction ratio in structural displacements (75.9%–92.7 %) although the mitigation effects in mitigating the structural bending moments turn to increase (4.1–38.9 %) due to
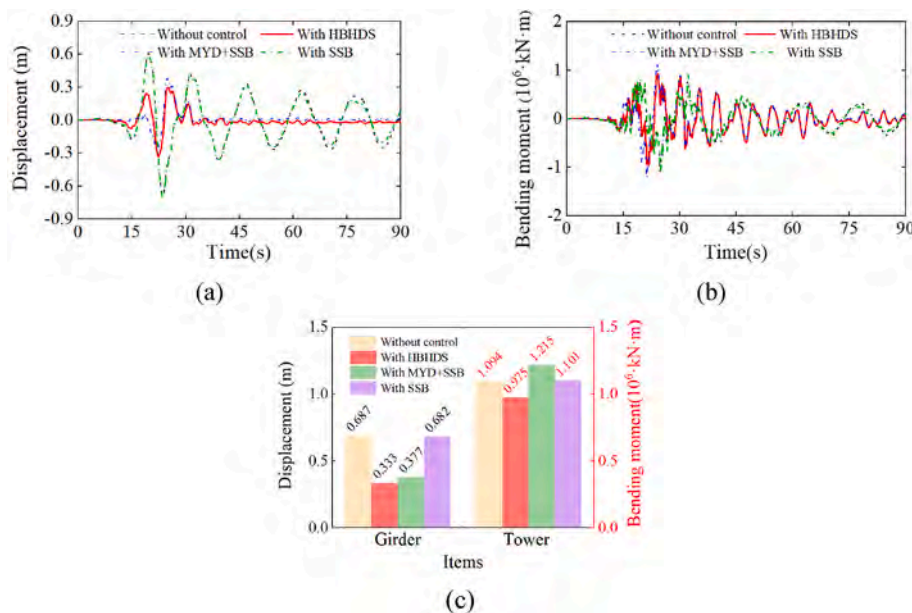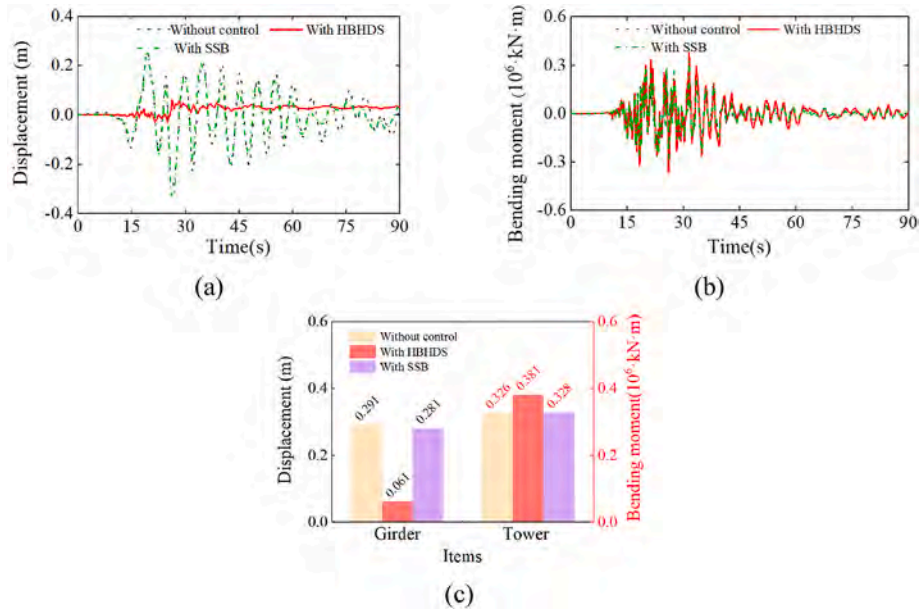

Fig. 17. The responses of the bridge with HBHDS considering the out-service dampers due to GM1 in the longitudinal direction: (a) girder-tower relative displacement, (b) bending moment at the base of the bridge tower, and (c) maximum seismic responses.

Table 8

Effect of HBHDS considering the out-of-service dampers on the maximum seismic responses of the bridge in the longitudinal direction.

Case	1	2	3	4
	Without control	With HBHDS	With MYD + SSB	With SSB
D_{L-max} (m)	0.687 (/)	0.332 (51.6 %)	0.377 (45.1 %)	0.682 (0.7 %)
M_{L-max} (10^6 kN·m)	1.094 (/)	0.976 (10.8 %)	1.215 (−11.1 %)	1.101 (−0.6 %)

Note: values in the ( ) denote the reduction ratio compared to the uncontrolled case (case 1).

Fig. 18. The responses of the bridge with HBHDS considering the out-of-service dampers due to GM 1 in the transverse direction: (a) girder-tower relative displacement, (b) bending moment at the base of the bridge tower, and (c) maximum seismic responses.

Table 9

Effect of HBHDS considering the out-of-service dampers on the maximum bridge seismic responses in the transverse direction.

Case	1	2	3
	Without control	With HBHDS	With SSB
D_{T-max} (mm)	0.291 (/)	0.061 (79.0 %)	0.281 (3.4 %)
M_{T-max} (10^6 kN·m)	0.326 (/)	0.381 (−16.5 %)	0.328 (−0.36 %)

Note: values in the ( ) denote the reduction ratio compared to the uncontrolled case (case 1).

the supplemental stiffness compared with the uncontrolled case; however, compared to the fixed system (FS) of the as-built bridge, HBHDS can moderately mitigate bending moments at the base of the bridge tower.

(3) HBHDS presents superior robustness to considering out-of-service dampers in terms of response reduction and energy dissipation capacity when subjected to NF pulse-like ground motions.

It is noteworthy that the simplified finite element model of the long-span bridge was mainly established considering a limited number of nonlinearities in the model (devices, cables). However, for a deeper investigation of the seismic behavior of the bridge, a more refined nonlinear approach could be required to be implemented. E.g., geometric nonlinearities could also play a role at different loading conditions. Indeed, investigating the performance of the proposed system under different loading conditions or structural configurations is in the future scope of the authors (e.g., long-term performance and durability under real-world conditions, material degradation, wear and tear, environmental exposure, and climate change).
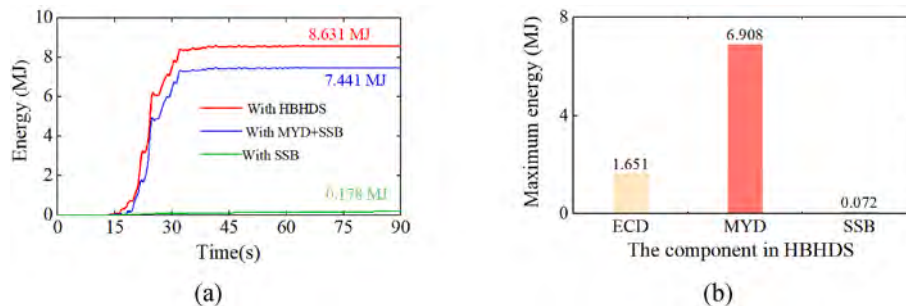
Fig. 19. Cumulative energy of HBHDS due to GM 1 in the longitudinal direction: (a) HBHDS considering the out-of-service dampers and (b) the maximum cumulative energy dissipation of each component in HBHDS without any failure.
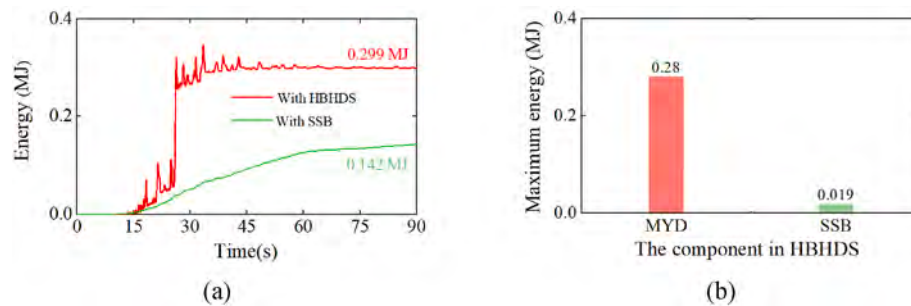
Fig. 20. Cumulative energy of HBHDS due to GM 1 in the transverse direction: (a) HBHDS considering the out-of-service dampers and (b) the maximum cumulative energy dissipation of each component in HBHDS without any failure.

CRediT authorship contribution statement

Renkang Hu: Writing – review & editing, Writing – original draft, Visualization, Validation, Software, Methodology, Investigation, Formal analysis, Data curation. **Menggang Yang:** Writing – review & editing, Project administration, Methodology, Funding acquisition, Conceptualization. **Dongliang Meng:** Writing – review & editing, Validation, Funding acquisition. **Raffaele Cucuzza:** Supervision. **Marco Domaneschi:** Writing – review & editing, Supervision, Project administration, Methodology, Funding acquisition, Conceptualization.

Declaration of competing interest

The authors declare that they have no known competing financial interests or personal relationships that could have appeared to influence the work reported in this paper.

Data availability

Data will be made available on request.

Acknowledgment

References

[1] Zheng SX, Shi XH, Jia HY, Zhao CH, Qu HL, Shi XL. Seismic response analysis of long-span and asymmetrical suspension bridges subjected to near-fault ground motion. Eng Fail Anal 2020;115:104615. https://doi.org/10.1016/j.engfailanal.2020.104615.
[2] Somerville PG, Smith NF, Graves RW, Abrahamson NA. Modification of empirical strong ground motion attenuation relations to include the amplitude and duration effects of rupture directivity. Seismol Res Lett 1997;68(1):199–222. https://doi.org/10.1785/gssrl.68.1.199.
[3] Malhotra P. Response of buildings to near-field pulse like ground motions. Earthq Eng Struct Dynam 1999;28(11):1309–26. https://doi.org/10.1002/eqe.4290240205.
[4] Snæbjörnsson JT, Sigtryggsdóttir FG, Sigbjörnsson R. Soil-structure interaction effects on the excitation and response of a low-rise RC building subjected to near- and far-fault earthquakes. In: Proceeding of the 15th world conference on earthquake engineering; 2012. Lisbon, Portugal. 2012.
[5] Broderick BM, Elnashai AS. Analysis of the failure of Interstate 10 freeway ramp during the Northridge earthquake of 17 January 1994. Earthq Eng Struct Dynam 1995;24(2):189–208. https://doi.org/10.1002/eqe.4290240205.
[6] Lu CH, Liu KY, Chang KC. Seismic performance of bridges with rubber bearings: lessons learnt from the 1999 Chi-Chi Taiwan earthquake. J Chin Inst Eng 2011;34(7):889–904. https://doi.org/10.1080/02533839.2011.591920.
[7] Wang Z, Lee GC. A comparative study of bridge damage due to the Wenchuan, Northridge, Loma Prieta and San Fernando earthquakes. Earthq Eng Eng Vib 2009;8:251–61. https://doi.org/10.1007/s11803-009-9063-y.
[8] Paudel J, Ryu H. Natural disasters and human capital: the case of Nepal's earthquake. World Dev 2018;111:1–12. https://doi.org/10.1016/j.worlddev.2018.06.019.
[9] Hu RK, Hu ST, Yang MG, Zhang Y. Metallic yielding dampers and fluid viscous dampers for vibration control in civil engineering: a review. Int J Struct Stabil Dynam 2022;22(16):2230006. https://doi.org/10.1142/S0219455422300063.
[10] Fujino Y, Siringoringo D. Vibration mechanisms and controls of long-span bridges: a review. Struct Eng Int 2013;23(3):248–68. https://doi.org/10.2749/101686613X13439149156886.
[11] De Domenico D, Ricciardi G, Takewaki I. Design strategies of viscous dampers for seismic protection of building structures: a review. Soil Dynam Earthq Eng 2019;118:144–65. https://doi.org/10.1016/j.soildyn.2018.12.024.
[12] Wesolowsky MJ, Wilson JC. Seismic isolation of cable-stayed bridges for near-field ground motions. Earthq Eng Struct Dynam 2003;32(13):2107–26. https://doi.org/10.1002/eqe.318.
[13] Yi J, Li JZ, Guan ZG. Shake table studies on viscous dampers in seismic control of a single-tower cable-stayed bridge model under near-field ground motions. J Earthq Tsunami 2018;12(5):1850011. https://doi.org/10.1142/S1793431118500112.
[14] Hu ST, Meng DL, Yang MG, Hu RK. Parametric optimization of the eddy current dampers applied to a suspension bridge considering bi-directional earthquakes. J Vib Control 2023;170853488. https://doi.org/10.1177/10775463231161456.
[15] Vargas R, Bruneau M. Effect of supplemental viscous damping on the seismic response of structural systems with metallic dampers. J Struct Eng 2007;133(10):1434–44. https://doi.org/10.1061/(ASCE)0733-9445(2007)133:10(1434).
[16] Arvind R, Santhi MH. A state of art review on hybrid passive energy dissipating devices. J Vib Eng Technol 2022;10(5):1931–54. https://doi.org/10.1007/s42417-022-00492-1.
[17] Stanikzai MH, Elias S, Chae Y. Recent advances in hybrid vibration-control systems. Pract Per on Struct Des Constr 2022;27(3):03122003. https://doi.org/10.1061/(ASCE)SC.1943-5576.0000685.
[18] Liang LT, Feng ZQ, Xu Y, Chen ZQ, Liang L. A parallel scheme of friction dampers and viscous dampers for girder-end longitudinal displacement control of a long-span suspension bridge under operational and seismic conditions. Build 2023;13:412. https://doi.org/10.3390/buildings13020412.
[19] Hu ST, Meng DL, Hu RK, Yang MG. A Combined Viscous-Steel Damping System (CVSDS) for longitudinal vibration mitigation of a long-span railway suspension bridge. J Earthq Eng 2023;27:1261–80. https://doi.org/10.1080/13632469.2022.2074915.
[20] Hu ST, Hu RK, Yang MG, Wang T. Seismic behavior of the combined viscous-steel damping system for a long-span suspension bridge considering wave-passage effect. J Bridge Eng 2023;28:04023034. https://doi.org/10.1061/JBENF2.BEENG-5718.
[21] Hu RK, Hu ST, Yang MG, Meng DL. Experimental study on the coordinated behavior of the Combined Viscous-Steel Damping System (CVSDS) for multi-level seismic mitigation. Structures 2023;57:105344. https://doi.org/10.1016/j.istruc.2023.105344.
[22] Yi J, Zhou JY, Ye XJ. Seismic control of cable-stayed bridge using negative stiffness device and fluid viscous damper under near-field ground motions. J Earthq Eng 2022;26:42–59. https://doi.org/10.1080/13632469.2020.1785588.
[23] Guan ZG, You H, Li JZ. An effective lateral earthquake-resisting system for long-span cable-stayed bridges against near-fault earthquakes. Eng Struct 2019;196:109345. https://doi.org/10.1016/j.engstruct.2019.109345.
[24] Guan ZG, Li JZ, Qu HY. Shake table test and numerical study on a capable and resilient lateral seismic isolation system for long-span cable-stayed bridges. Soil Dynam Earthq Eng 2023;164:107629. https://doi.org/10.1016/j.soildyn.2022.107629.
[25] Zhou LX, Wang XW, Ye AJ. Shake table test on transverse steel damper seismic system for long span cable-stayed bridges. Eng Struct 2019;179:106–19. https://doi.org/10.1016/j.engstruct.2018.10.073.
[26] Li S, Dezfuli FH, Wang JQ, Alam MS. Longitudinal seismic response control of long-span cable-stayed bridges using shape memory alloy wire-based lead rubber bearings under near-fault records. J Intell Mater Syst Struct 2018;29(5):703–28. https://doi.org/10.1177/1045389X17721030.
[27] Hui YX, Li LS, Cheng H, Zhang YJ, Wang DS. Seismic mitigation of continuous girder bridges equipped with U-shaped stainless steel dampers under near-fault earthquake excitations. Structures 2023;58:105597. https://doi.org/10.1016/j.istruc.2023.105597.

[28] Elias S, Djerouni S. Optimum tuned mass damper inerter under near-fault pulse-like ground motions of buildings including soil-structure interaction. J Build Eng 2024;108674. https://doi.org/10.1016/j.jobe.2024.108674.

[29] Hu ST, Yang MG, Meng DL, Hu RK. Damping performance of the degraded fluid viscous damper due to oil leakage. Structures 2023;16:9–19. https://doi.org/10.1016/j.istruc.2023.01.070.

[30] Hu ST, Hu RK, Yang MG, Wang T. Seismic performance of the combined viscous-steel damping system suffering from oil leakage. J Vib Control 2023;29:4885–95. https://doi.org/10.1177/10775463221126028.

[31] Yang MG, Hu RK, Meng DL, Zhang HJ. A novel Horizontal Bidirectional Hybrid Damping System (HBHDS) for multi-level vibration control of long-span bridges: a theoretical study. Eng Struct 2024;305:117693. https://doi.org/10.1016/j.engstruct.2024.117693.

[32] Guo T, Liu J, Zhang YF, Pan SJ. Displacement monitoring and analysis of expansion joints of long-span steel bridges with viscous dampers. J Bridge Eng 2015;20:04014099. https://doi.org/10.1061/(ASCE)BE.1943-5592.0000701.

[33] Ismail M, Casas JR, Rodellar J. Near-fault isolation of cable-stayed bridges using RNC isolator. Eng Struct 2013;56:327–42. https://doi.org/10.1016/j.engstruct.2013.04.007.

[34] Ernst H. Der E-modul von seilen unter bercksichtigung des durchhanges. Bauingenieur 1965;40(2):52–5.

[35] Wang H, Hu RM, Xie J, Tong T, Li AQ. Comparative study on buffeting performance of Sutong Bridge based on design and measured spectrum. J Bridge Eng 2013;18:587–600. https://doi.org/10.1061/(ASCE)BE.1943-5592.0000394.

[36] Park JG, Otsuka H. Optimal yield level of bilinear seismic isolation devices. Earthq Eng Struct Dynam 1999;28(9):941–55. https://doi.org/10.1002/(SICI)1096-9845(199909)28:9%3C941::AID-EQE848%3E3.0.CO;2-5.

[37] Wouterse JH. Critical torque and speed of eddy current brake with widely separated soft iron poles. IEE Process B 1991;138:153–8. https://doi.org/10.1049/ip-b.1991.0019.

[38] Liang LT, Feng ZQ, Chen ZQ. Seismic control of SDOF systems with nonlinear eddy current dampers. Appl Sci 2019;9(16):3427. https://doi.org/10.3390/app9163427.

[39] Makris N, Burton SA, Hill D, Jordan M. Analysis and design of ER damper for seismic protection of structures. J Eng Mech 1996;122(10):1003–11. https://doi.org/10.1061/(ASCE)0733-9399(1996)122:10(1003).

[40] Chioccarelli E, Iervolino I. Near-source seismic demand and pulse-like records: a discussion for L'Aquila earthquake. Earthq Eng Struct Dynam 2010;39(9):1039–62. https://doi.org/10.1002/eqe.987.

[41] Ministry of Transport of the People's Republic of China. JTG/T 2231-01-2020 Specifications for seismic design of Highway bridges. Beijing, China: China Communications Press; 2020 [in Chinese].

[42] Pacor F, Felicetta C, Lanzano G, Sgobba S, Puglia R, D'Amico M, Russo E, Baltzopoulos G, Iervolino I. NESS v1.0: a worldwide collection of strong-motion data to investigate near source effects. Seismol Res Lett 2018;89(6):2299–313. https://doi.org/10.1785/0220180149.

[43] Wolff ED, Ipek C, Constantinou MC, Tapan M. Effect of viscous damping devices on the response of seismically isolated structures. Earthq Eng Struct Dynam 2015;44(2):185–98. https://doi.org/10.1002/eqe.2464.

[44] Li S, Zhang F, Wang JQ, Alam MS, Zhang J. Effects of near-fault motions and artificial pulse-type ground motions on super-span cable-stayed bridge systems. J Bridge Eng 2017;22(3):04016128. https://doi.org/10.1061/(ASCE)BE.1943-5592.0001008.

[45] Starossek U, Haberland M. Approaches to measures of structural robustness. Struct Infrastruct Eng 2011;7(7–8):625–31. https://doi.org/10.1080/15732479.2010.501562.

[46] Das S, Chakraborty S, Chen Y, Tesfamariam S. Robust design optimization for SMA based nonlinear energy sink with negative stiffness and friction. Soil Dynam Earthq Eng 2021;140:106466. https://doi.org/10.1016/j.soildyn.2020.106466.

[47] Domaneschi M, Martinelli L, Po E. Control of wind buffeting vibrations in a suspension bridge by TMD: hybridization and robustness issues. Comput Struct 2015;155:3–17. https://doi.org/10.1016/j.compstruc.2015.02.031.